

Liquid-nitrogen-jet laser-plasma source for compact soft x-ray microscopy

P. A. C. Jansson,^{a)} U. Vogt, and H. M. Hertz

Biomedical and X-Ray Physics, Royal Institute of Technology/Albanova, SE-106 91 Stockholm, Sweden

(Received 14 December 2004; accepted 30 January 2005; published online 23 March 2005)

We describe a liquid-nitrogen-jet laser-plasma source with sufficient brightness, uniformity, stability, and reliability to be suitable for compact water-window soft x-ray transmission microscopy. A cooled capillary nozzle arrangement allows long-term operation and avoids previously reported jet instabilities. The source is quantitatively characterized by calibrated slit-grating spectroscopy and zone-plate imaging. The absolute photon number in the major spectral lines ($\lambda=2.48$ nm and $\lambda=2.88$ nm) is 1.0×10^{12} photons/(pulse \times sr \times line). The source diameter is ~ 20 μ m (full width at half maximum) and the spatial stability is better than ± 2 μ m. Within an area with uniformity of 20%, the average source brightness is 4×10^8 photons/(pulse \times sr \times μ m² \times line), which allows operation of a compact soft x-ray transmission microscope with exposure times of a few minutes. © 2005 American Institute of Physics. [DOI: 10.1063/1.1884186]

I. INTRODUCTION

Soft x-ray microscopy in the water-window ($\lambda=2.3$ – 4.4 nm) exploits the natural contrast between carbon and oxygen for high-resolution imaging of, e.g., unstained biological samples.¹ Present compact soft x-ray microscopes operate at $\lambda=3.37$ nm using a methanol or ethanol liquid-jet laser-plasma source.² However, imaging of thicker (~ 10 μ m) objects, e.g., typical mammalian cells, requires operation in the lower part of the water-window where the transmission is higher. In the present paper we demonstrate a $\lambda=2.48$ nm liquid-nitrogen-jet laser-plasma source with sufficient brightness, stability, and reliability for operation in a compact soft x-ray transmission microscope.

Most present soft x-ray microscopes are based on high-brightness synchrotron-radiation sources. Typically they operate at $\lambda=2.4$ nm, close to the oxygen *K*-absorption edge, in order to minimize oxygen absorption thereby enabling imaging of thick samples with short exposure times. However, the limited accessibility to synchrotron-radiation-based instruments reduces the impact of x-ray microscopy as an important tool for user-motivated research. Therefore we developed a compact x-ray microscope operating in the water-window.³ The microscope is based on a micro zone plate objective, a normal incidence multilayer-mirror condenser, and a CCD detector in combination with a liquid-jet laser-plasma source. At present, the target material is methanol resulting in hydrogenlike carbon emission at $\lambda=3.37$ nm. The microscope has demonstrated suboptical resolution (approx. 50 nm) on test samples as well as imaging of thin (1–2 μ m) unstained cells. The instrument requires a stable source with high brightness for reasonable exposure times.

Liquid-jet laser plasmas^{4,5} are attractive, compact, high brightness sources for x-ray and extreme ultraviolet (EUV) radiation. They offer reliable, spatially well defined, regen-

erative sources allowing high-repetition-rate operation with minimum debris emission.⁶ By choosing a suitable target liquid and correct plasma conditions, the emission wavelength may be spectrally tailored to suit different applications, e.g., water,^{7,8} xenon,^{9,10} and tin^{11,12} for ~ 0.1 keV EUV lithography, ethanol,⁴ methanol,¹³ ammonium hydroxide,¹⁴ liquid nitrogen,¹⁵ and argon¹⁶ for ~ 1 keV soft x-ray microscopy and reflectometry, and gallium¹⁷ and copper solutions¹⁸ for ~ 10 keV hard x-ray diffraction experiments.

Hydrogenlike and heliumlike nitrogen ions emit strongly at $\lambda=2.478$ nm (*Ly- α*) and $\lambda=2.879$ nm (*He- α*), making nitrogen an attractive target for soft x-ray microscopy in the lower part of the water-window. Nitrogen benefits from being relatively inert, thereby minimizing damage of and deposition on sensitive x-ray optics due to debris. Compared to the use of, e.g., ammonium hydroxide¹⁴ as the nitrogen-containing target liquid, the higher nitrogen content of liquid nitrogen both offers the possibility to generate single-element emission and more effective conversion from laser energy to useful x-ray flux.¹⁹ However, previous attempts to produce liquid-nitrogen jets in vacuum have been hampered by instabilities^{15,16} making them unsuitable for laser-plasma applications such as microscopy which require a stable source.

We are presently developing a compact soft x-ray microscope for operation at $\lambda=2.48$ nm using a liquid-nitrogen-jet laser-plasma source. This microscope will be based on a zone-plate condenser²⁰ since present normal-incidence multilayer mirrors for this wavelength neither have the required reflectivity nor the necessary uniformity. In the present paper we investigate the liquid-nitrogen-jet laser-plasma source and its applicability to x-ray microscopy. With a new nozzle design we find that the temporal and spatial stability as well as the reliability is sufficient for x-ray microscopy use. Furthermore, we quantitatively measure flux, brightness, and source size. These are key parameters when designing x-ray optical systems, such as the x-ray microscope.

^{a)}Electronic mail: per.jansson@biox.kth.se

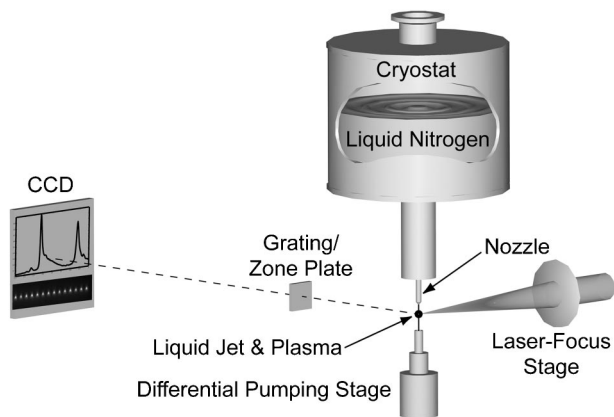


FIG. 1. Experimental arrangement.

II. EXPERIMENTAL ARRANGEMENT

Figure 1 depicts the experimental arrangement. It consists of a vacuum chamber, a target delivery system, a laser-focus system, a slit grating spectrograph, and a zone plate imaging arrangement.

The liquid-nitrogen target delivery system employs a fused silica capillary which is pulled into a taper and polished to an $\sim 18 \mu\text{m}$ diameter orifice.²¹ Up to 60 bars of nitrogen pressure is applied to the capillary, which is lead into the vacuum chamber via a liquid-nitrogen-filled cryostat, providing on-line cooling and liquidification of the applied nitrogen gas. The resulting liquid-nitrogen jet enters the vacuum chamber with a speed up to $\sim 100 \text{ m/s}$. After 5 mm of free flight the jet enters a differential-pumping stage kept at $\sim 1 \text{ mbar}$. This enables operation of jet diameters up to $20 \mu\text{m}$ while still maintaining 10^{-3} mbar within the main chamber using an 880 l/s turbo-drag pump. By reducing the pressure inside the liquid-nitrogen cryostat to $\sim 150 \text{ mbar}$, evaporative cooling lowers the temperature of the reservoir to the desired 64 K optimal for stable jet operation.²² Stable jet operation is further facilitated by purifying the nitrogen gas supply using a molecular sieve filter immersed in liquid nitrogen in combination with a stainless steel sintered filter. The resulting angular instability of the jet is $< 1 \text{ mrad}$. Previously reported instabilities^{15,16} are not observed. Furthermore, the system routinely allows long-term operation without interrupts.

The plasma is generated by a pulsed, 100 Hz, $\sim 3 \text{ ns}$, frequency-doubled Nd:YAG laser (Coherent Infinity 40-100). The beam is focused with a $\sim 150 \text{ mm}$ focal length lens and aligned to the continuous part of the jet using an x-y-z laser-focus stage capable of positioning the focus with an accuracy of $\sim 0.5 \mu\text{m}$. Simulations of the optical system give a laser full-width-at-half-maximum (FWHM) diameter of $14 \mu\text{m}$ in the focus, which agrees well with knife edge scan measurements ($\sim 15 \mu\text{m}$). Pulse energies up to $\sim 200 \text{ mJ}$, corresponding to focal intensities of $\sim 4 \times 10^{13} \text{ W/cm}^2$, can be achieved at the liquid-nitrogen jet target. The pulse-to-pulse stability of the laser is $\sim 7\%$ (1σ) when operating at 200 mJ. A chromium-filtered photodiode enables real-time monitoring of the plasma x-ray emission.

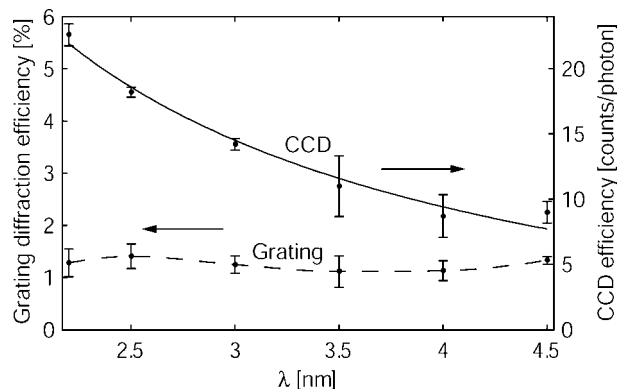


FIG. 2. Calibration curves obtained at the ELSA synchrotron radiation facility. Left scale: measured grating diffraction efficiency and experimental fit. Right scale: measured CCD efficiency and data fit to theoretical shape.

The jet and plasma are also monitored at visible wavelengths by a CCD detector attached to a long-working-distance $12 \times$ zoom microscope.

Emission spectra and quantitative flux measurements were performed with a slit-grating spectrograph.²³ It employs a free-standing transmission grating, made of gold on a silicon substrate, with 10 000 lines/mm and a total width of $120 \mu\text{m}$. The grating was positioned 658 mm away from the laser plasma in the direction orthogonal to the laser beam. Low-energy radiation and stray light from the laser was blocked by a $\sim 300 \text{ nm}$ thick chromium filter. The $300 \mu\text{m}$ height of the grating in combination with a rectangular entrance slit of $52 \mu\text{m}$ width in front of the grating led to a collected solid angle of $3.6 \times 10^{-8} \text{ sr}$ for the spectrograph. The distance from the grating to the x-ray-sensitive CCD detector (Photometrics CH350 with SITE SI003AB chip) was 672 mm. With this geometry, the arrangement results in a spectral resolution of $\lambda/\Delta\lambda > 80$ @ $\lambda = 2.48 \text{ nm}$, for a source size $< 100 \mu\text{m}$.²³ Absolute calibration of the filter transmission and the grating and CCD efficiency was performed at the ELSA synchrotron radiation facility in Bonn. Figure 2 shows the absolute efficiency for the grating and the CCD. Based on the calibration process, we determine that the systematic error in the spectral flux measurements performed with the system is less than 30%.

Source size, emission distribution, brightness and stability were determined with a zone-plate imaging arrangement. A 5-mm diameter condenser zone plate (CZP) (Ref. 20) is combined with a central stop to form a magnified image of the source on the CCD detector. Due to the large numerical aperture of the CZP, it is possible to perform single-shot imaging. Furthermore, since the focal length of the CZP is wavelength dependent, the arrangement acts as a linear monochromator enabling wavelength-selective imaging of the plasma.²⁴ Calibration of the zone-plate efficiency was performed by Rehbein *et al.*²⁰ resulting in an absolute efficiency of 7.0% at $\lambda = 2.478 \text{ nm}$ and 5.1% at $\lambda = 2.879 \text{ nm}$. The focal length in the first diffraction order is 90 mm at $\lambda = 2.478 \text{ nm}$, and 77.5 mm at $\lambda = 2.879 \text{ nm}$. The image was brought into focus by keeping the distance from CZP to CCD constant at $\sim 1948 \text{ mm}$, while adjusting the distance from plasma to CZP. This yields a magnification of ~ 21 for λ

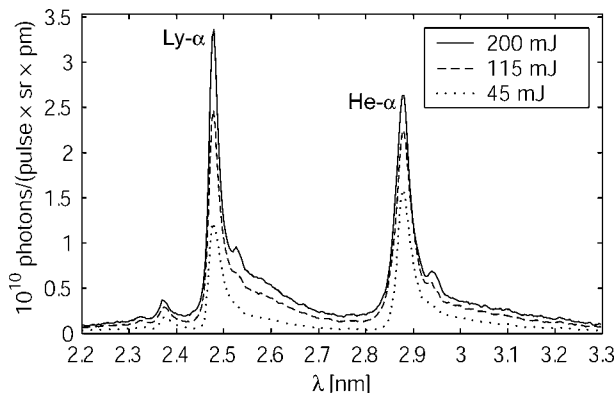


FIG. 3. Liquid-nitrogen-jet laser-plasma emission spectra for three different laser-pulse energies.

$\lambda=2.478$ nm and ~ 24 for $\lambda=2.879$ nm. At these magnifications and with a pixel size of $24 \mu\text{m}$, the corresponding spatial resolution in the source plane is $2.3 \mu\text{m}$ and $2 \mu\text{m}$, respectively. For the same reasons as when performing spectroscopy, chromium filters were used at $\lambda=2.478$ nm and chromium in combination with titanium at $\lambda=2.879$ nm. By combining the uncertainties in source size data, filter transmission and the quantum efficiency of the CZP, the systematic error in the brightness measurements is estimated to be less than 40%.

III. RESULTS AND DISCUSSION

All measurements have been performed at three different laser-pulse energies, 45, 115, and 200 mJ of $\lambda=532$ nm in the focus. The results presented below are averages over many experiments, with special emphasis on source characteristics important when using the source for soft x-ray microscopy operating at $\lambda=2.48$ nm.

Figure 3 shows the quantitative laser-plasma emission spectra for the three different laser pulse energies. The spectra were recorded at maximum x-ray flux for each laser energy and optimal plasma conditions were found by running the CCD detector in “focus mode” (rapid exposure and readout), while adjusting the laser focus position. The spectra were then recorded with 500–2000 laser shots. The total flux in a single emission line can be calculated by integrating the spectra from $\lambda_0 - \Delta\lambda$ to $\lambda_0 + \Delta\lambda$. Here λ_0 is the peak wavelength and $\Delta\lambda$ is the resolution of the spectrograph, which approximately determines the recorded line width in these measurements. Given the $\sim 100 \mu\text{m}$ full width at $\sim 10\%$ of maximum (cf. below), the spectral resolution is $\Delta\lambda = 0.032$ nm. Using this integration interval, $\sim 1.0 \times 10^{12}$ photons/(pulse \times sr \times line) in each of the two emission lines was obtained with 200 mJ/pulse laser energy. This corresponds to a conversion efficiency of $\sim 0.5\%$ assuming 4π sr isotropic emission. Table I shows the x-ray flux and its dependence on laser pulse energy for the two emission lines. The measured flux compares well with previous work.^{15,16,25}

In order to measure shot-to-shot source size, brightness, and stability we recorded several single-shot images of the source in one detector exposure. This was accomplished by leaving the CCD detector shutter open after a 40 ms exposure. During readout of the CCD chip, the laser hit the target

TABLE I. X-ray flux from nitrogen line emission.

E_{pulse} (mJ)	I_{Focus} (W/cm^2)	$\lambda=2.48$ nm [photons/(pulse \times sr \times line)]	$\lambda=2.28$ nm [photons/(pulse \times sr \times line)]
45	8.2×10^{12}	4.0×10^{11}	5.7×10^{11}
115	2.2×10^{13}	7.9×10^{11}	9.1×10^{12}
200	3.7×10^{13}	1.0×10^{12}	1.0×10^{12}

at a frequency of 5 Hz, thereby exposing the chip with each single-shot image. This results in a CCD recording where the different single-pulse images are geometrically separated from each other. Figure 4 shows a part of such a multiexposed CCD recording with nine single-shot plasmas at $\lambda=2.48$ nm. The horizontal line plot in the bottom is a vertical integration of the recorded intensity. The advantage of this method is that it enables recording of up to 20 successive single-pulse images in one image file, each of them providing shot-to-shot information of source size and brightness. Furthermore, by assuming that the readout speed and laser repetition rate is constant, the spatial stability of the plasma can be determined. In order to increase the accuracy, all results have been calculated using data from five image sets, corresponding to ~ 100 single-shot images, for each investigated pulse energy. Optimization of the laser focus position was performed using the detector in “focus mode,” with the aim of maximizing source brightness while keeping the source circular symmetric. Figure 5 shows the shape of a typical single-shot image at $\lambda=2.48$ nm using a laser pulse energy of 200 mJ.

After dark image subtraction, each plasma image was analyzed by two line plots in the horizontal and vertical directions through the pixel with maximum intensity. The full width at half maximum was used as a measure of the source size. Figure 6 illustrates the dependence of the source size on the laser pulse energy at $\lambda=2.48$ nm, where the bars indicating the variation (1σ) between individual shots. Note the asymmetry for low pulse energies. In contrast, the $\lambda=2.88$ nm data are symmetrical with FWHM $\sim 20 \mu\text{m}$ for all pulse energies investigated.

For the determination of the spatial stability, the position of the pixel with maximum intensity was used to calculate the shot-to-shot variation of the plasma position. It was

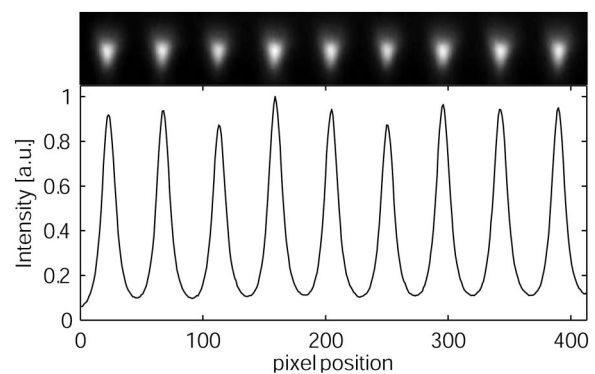


FIG. 4. Typical single-shot images and vertically integrated line plot along horizontal axis.

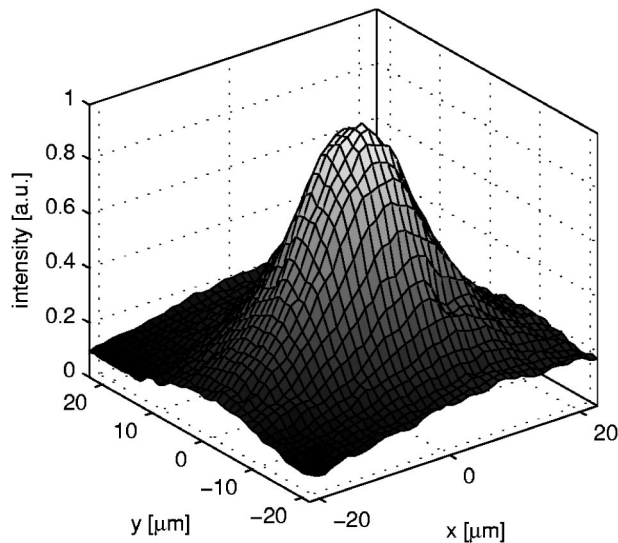


FIG. 5. Source shape at $\lambda=2.48$ nm using a laser pulse energy of 200 mJ.

found that the spatial stability for both spectral lines was ± 2 μm (1σ) horizontally, and ± 2 μm (1σ) vertically, independent of the laser pulse energy.

IV. APPLICABILITY TO SOFT X-RAY MICROSCOPY

The future compact soft x-ray microscope will employ a condenser zone plate (CZP) to illuminate the object in critical illumination via 1:1 imaging of the source into the object plane. It will utilize the same CZP as in the present paper. The key parameter for a transmission x-ray microscope is the brightness in the object-plane field of view. Due to the 1:1 imaging conditions the object-plane brightness is directly determined by the source brightness, defined as photons/(pulse \times sr \times μm^2 \times line). In addition, the object-plane field of view should be illuminated with reasonable uniformity to allow high-quality imaging over the full area. Should the full source of Fig. 5 be used for the illumination, imaging outside the center would be hampered by the low brightness. However, the hollow cone illumination of the CZP/central-field-stop arrangement in combination with the micro-zone plate imaging and CCD detector results in a field of view $\sim 12\mu\text{m}$ when operating the microscope at $1000\times$ magnification. The fact that the source is larger than the field of view results in that a fraction of the available photons in

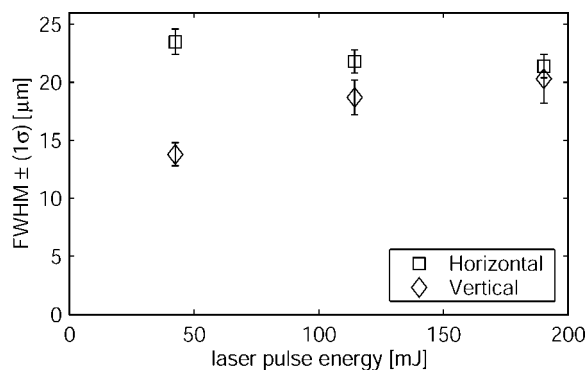


FIG. 6. The source size at $\lambda=2.48$ nm as function of the laser pulse energy. The bars indicate the 1σ variations.

TABLE II. Average source brightness and uniformity within the 12 μm field-of-view required for microscopy using the CZP as a condenser.

λ (nm)	E_{pulse} (mJ)	Brightness [photons/(pulse \times sr \times μm^2 \times line)]	Uniformity
2.48	45	1.7×10^8	0.33
2.48	115	2.9×10^8	0.23
2.48	190	4.1×10^8	0.19
2.88	45	1.1×10^8	0.29
2.88	115	3.3×10^8	0.26
2.88	195	4.4×10^8	0.24

this arrangement are lost in return for a more uniform illumination of the sample. We therefore characterize the expected illumination in the object plane by the average source brightness and the uniformity within this field of view. The illumination uniformity can be defined as $(I_{\text{max}} - I_{\text{min}})/(I_{\text{max}} + I_{\text{min}})$. Using this definition, a uniformity of zero corresponds to a perfectly uniform illumination.

Table II shows the average brightness and uniformity within a 12 μm field of view as a function of the laser pulse energy. The best source conditions were found using a 200 mJ pulse, which gives an average brightness of 4.1×10^8 photons/(pulse \times sr \times μm^2 \times line) with a uniformity of 19%. This corresponds to an average intensity of 1.0×10^5 photons/(s \times μm^2) in the object plane. Assuming a nickel micro zone plate with 7.6% efficiency operating at $\times 1000$ magnification and a CCD pixel size of 24 μm , this brightness enables recording of high quality images (~ 1000 photons/pixel) of dry samples with an exposure time below 4 min. The shot-to-shot variations of the brightness was found to be below 15% (1σ) which should be compared with the pulse-to-pulse stability of the laser at 7% (1σ). However, since each exposure is made up of many pulses (N), which reduce the variation from exposure to exposure by a factor of $1/N^{1/2}$, the statistical fluctuation between exposures will be very low.

Finally, the debris properties of the source must be considered. The source must not damage fragile optical components in its vicinity. Due to the relative inertness of nitrogen, damage and deposition due to atomic and ionic debris is negligible. However, particulate debris may pose a problem. Particulate debris was investigated by positioning a 250 nm thick Cr-filter approximately 180 mm away from the plasma, the same distance as in the future x-ray microscope. By using the visual plasma emission to back illuminate the foil while observing it through a microscope, the creation of pinholes can be detected. The filter was exposed to the plasma for 1 h without creation of detectable pinholes.

Although the present source already has the necessary properties for compact soft x-ray microscopy with reasonable exposure times, there is room for improvement. Of special importance are reduced exposure times. The target delivery system allows operation of much higher repetition-rate.⁸ Thus, e.g., a kHz laser with similar pulse energy as the present laser can be utilized, thereby increasing the average x-ray flux by an order of magnitude. This would translate into typical exposure times below 30 s.

ACKNOWLEDGMENTS

The authors gratefully acknowledge S. Rehbein and A. Holmberg for providing us with the condenser zone plate used in the experiments. This work has been supported by the Swedish Science Research Council and partly supported by Deutsche Forschungsgemeinschaft under Contract No. W1 1451/3-1. U. Vogt is grateful for the support from the Göran Gustafsson Foundation.

- ¹J. Kirz, C. Jacobsen, and M. Howells, *Q. Rev. Biophys.* **28**, 33 (1995).
- ²G. A. Johansson, A. Holmberg, H. M. Hertz, and M. Berglund, *Rev. Sci. Instrum.* **73**, 1193 (2002).
- ³M. Berglund, L. Rymell, M. Peuker, T. Wilhein, and H. M. Hertz, *J. Microsc. (Paris)* **197**, 268 (2000).
- ⁴L. Rymell and H. M. Hertz, *Opt. Commun.* **103**, 105 (1993).
- ⁵L. Malmqvist, L. Rymell, M. Berglund, and H. M. Hertz, *Rev. Sci. Instrum.* **67**, 4150 (1996).
- ⁶L. Rymell and H. M. Hertz, *Rev. Sci. Instrum.* **66**, 4916 (1995).
- ⁷H. M. Hertz, L. Rymell, M. Berglund, and L. Malmqvist, *Proc. SPIE* **2523**, 88 (1995).
- ⁸U. Vogt, H. Stiel, I. Will, P. V. Nickles, W. Sandner, M. Wieland, and T. Wilhein, *Appl. Phys. Lett.* **79**, 2336 (2001).
- ⁹B. A. M. Hansson, L. Rymell, M. Berglund, and H. M. Hertz, *Microelectron. Eng.* **53**, 667 (2000).
- ¹⁰T. Abe, T. Suganuma, Y. Imai, H. Someya, H. Hoshino, M. Nakano, G. Soumagne, H. Komori, Y. Takabayashi, H. Mizoguchi, A. Endo, K. Toyoda, and Y. Horiike, *Proc. SPIE* **5374**, 160 (2004).
- ¹¹P. A. C. Jansson, B. A. M. Hansson, O. Hemberg, M. Otendal, A. Holmberg, J. de Groot, and H. M. Hertz, *Appl. Phys. Lett.* **84**, 2256 (2004).
- ¹²M. Richardson, C. S. Koay, K. Takenoshita, C. Keyser, and M. Al Rabban, *J. Vac. Sci. Technol. B* **22**, 785 (2004).
- ¹³J. de Groot, O. Hemberg, A. Holmberg, and H. M. Hertz, *J. Appl. Phys.* **94**, 3717 (2003).
- ¹⁴L. Rymell, M. Berglund, and H. M. Hertz, *Appl. Phys. Lett.* **66**, 2625 (1995).
- ¹⁵M. Berglund, L. Rymell, H. M. Hertz, and T. Wilhein, *Rev. Sci. Instrum.* **69**, 2361 (1998).
- ¹⁶M. Wieland, T. Wilhein, M. Faubel, C. Eilert, M. Schmidt, and O. Sublemontier, *Appl. Phys. B: Lasers Opt.* **72**, 591 (2001).
- ¹⁷G. Korn, A. Thoss, H. Stiel, U. Vogt, M. Richardson, T. Elsaesser, and M. Faubel, *Opt. Lett.* **27**, 866 (2002).
- ¹⁸R. J. Tompkins, I. P. Mercer, M. Fettweis, C. J. Barnett, D. R. Klug, L. G. Porter, I. Clark, S. Jackson, P. Matousek, A. W. Parker, and M. Towrie, *Rev. Sci. Instrum.* **69**, 3113 (1998).
- ¹⁹T. Wilhein, D. Hambach, B. Niemann, M. Berglund, L. Rymell, and H. M. Hertz, *Appl. Phys. Lett.* **71**, 190 (1997).
- ²⁰S. Rehbein, A. Holmberg, G. A. Johansson, P. A. C. Jansson, and H. M. Hertz, *J. Vac. Sci. Technol. B* **22**, 1118 (2004).
- ²¹J. de Groot, G. A. Johansson, and H. M. Hertz, *Rev. Sci. Instrum.* **74**, 3881 (2003).
- ²²P. A. C. Jansson, Master thesis, Biomedical and X-Ray Physics, Physics, KTH, Stockholm, 2002.
- ²³T. Wilhein, S. Rehbein, D. Hambach, M. Berglund, L. Rymell, and H. M. Hertz, *Rev. Sci. Instrum.* **70**, 1694 (1999).
- ²⁴U. Vogt, R. Frueke, T. Wilhein, H. Stollberg, P. A. C. Jansson, and H. M. Hertz, *Appl. Phys. B: Lasers Opt.* **78**, 53 (2004).
- ²⁵M. Wieland, U. Vogt, M. Faubel, T. Wilhein, D. Rudolph, and G. Schmahl, *AIP Conf. Proc.* **507**, 726 (2000).